**Proceedings of the ASME 2020
Dynamic Systems and Control Conference
DSCC2020
October 5-7, 2020, Virtual, Online**

DSCC2020-3190

HIERARCHICAL MULTI-TIMESCALE ENERGY MANAGEMENT FOR HYBRID-ELECTRIC AIRCRAFT

Wenqing Wang
Department of Mechanical Engineering
University of Texas at Dallas
Richardson, Texas, 75080
Wenqing.Wang@UTDallas.edu

Justin P. Koeln*
Department of Mechanical Engineering
University of Texas at Dallas
Richardson, Texas, 75080
Justin.Koeln@UTDallas.edu

ABSTRACT

Hybrid-electric aircraft represent an important step in the transition from conventional fuel-based propulsion to fully-electric aircraft. For hybrid power systems, overall aircraft performance and efficiency highly depend on the coordination of the fuel and electrical systems and the ability to effectively control state and input trajectories at the limits of safe operation. In such a safety-critical application, the chosen control strategy must ensure the closed-loop system adheres to these operational limits. While hierarchical Model Predictive Control (MPC) has proven to be a computationally efficient approach to coordinated control of complex systems across multiple timescales, most formulations are not supported by theoretical guarantees of actuator and state constraint satisfaction. To provide guaranteed constraint satisfaction, this paper presents set-based hierarchical MPC of a 16 state hybrid-electric aircraft power system. Within the proposed two-level vertical hierarchy, the long-term control decisions of the upper-level controller and the short-term control decisions of the lower-level controller are coordinated through the use of waysets. Simulation results show the benefits of this coordination in the context of hybrid-electric aircraft performance and demonstrate the practicality of applying set-based hierarchical MPC to complex multi-timescale systems.

1 INTRODUCTION

In the transition from conventional fuel-based propulsion to fully-electric aircraft, hybrid-electric aircraft combine the high specific energy storage of fuel with the increased efficiency of power electronics. With increasing demands for both performance and efficiency, the generation, conversion, storage, and utilization of energy must be coordinated across energy domains, vehicle subsystems, and timescales. Moreover, due to the safety critical nature of aircraft, this coordination must produce provably safe system trajectories that are guaranteed to satisfy all input and state constraints for the duration of operation.

With a rich supporting theory, Model Predictive Control (MPC) [1] is well-suited to enforce input and state constraints and to leverage preview of known flight-plan information within the prediction horizon. Therefore, there is an extensive ongoing effort to develop control-oriented models of aircraft power systems [2–6] along with centralized [7–9] and distributed [10–12] MPC formulations that leverage these models.

However, centralized and distributed MPC formulations may become computationally intractable when combining the fast control update rates required to resolve fast timescale dynamics with the long prediction horizons needed to optimize slow timescale dynamics over the course of a several hour long flight. Alternatively, hierarchical MPC is specifically designed to achieve computationally-efficient control of multi-timescale systems. Through both simulation and Hardware-In-the-Loop (HIL) experiments, hierarchical MPC has been demonstrated to provide improved temporal and functional coordination among electrical and thermal subsystems resulting in greater system performance, reduced constraint violations, and increased system efficiency [13–15]. In these application-oriented hierarchical MPC formulations, coordination is achieved through communicating

*Address all correspondence to this author.

state and input trajectories determined by upper-level controllers down the hierarchy as references to be tracked by lower-level controllers. With proper cost function tuning, this reference-tracking based approach can achieve the desired closed-loop performance in practice.

Unlike centralized MPC, reference-tracking based hierarchical MPC does not have the supporting control theory needed to guarantee closed-loop constraint satisfaction. For safety critical applications like aircraft, set-based hierarchical MPC has been developed in [16, 17], where coordination between controllers is achieved through the use of waysets as an alternative to reference-tracking. For a vertical hierarchy, with one controller per level, the nominal set-based hierarchical MPC formulation from [16] was extended in [17] to include robustness to bounded, unknown disturbances. Unlike reference-tracking, wayset-based coordination leverages reachability analysis, allowing lower-level controllers the flexibility to use the fast dynamics of the system to improve system performance while still providing guaranteed constraint satisfaction.

This paper demonstrates the benefits of set-based hierarchical MPC when applied to the energy management of hybrid-electric aircraft with respect to provable constraint satisfaction and practical improvements to overall aircraft performance. Previously, set-based hierarchical MPC has only been applied to systems with a relatively few number of states with short operating duration [16, 17]. Thus, key contributions of this paper are the practical formulation and demonstration of set-based hierarchical MPC to a more complex system with multi-timescale dynamics. Moreover, simulation results clearly show how the performance of hybrid-electric aircraft is highly dependent on the effective coordination of both long- and short-term energy management.

The remainder of the paper is organized as follows. Section 2 introduces the specific power system architecture and graph-based dynamic model used to capture the key features of the more general class of hybrid-electric aircraft. A two-level set-based hierarchical MPC formulation is presented in Section 3 including the individual controller formulations and the zonotope-based method for computing the waysets used to coordinate these controllers. Section 4 presents the simulation-based results that demonstrate the practicality and benefits achieved using set-based hierarchical MPC for the energy management of hybrid-electric aircraft. Finally, Section 5 summarizes the conclusions of the paper and provides future research directions.

2 HYBRID-ELECTRIC AIRCRAFT MODELING

2.1 Candidate Power System Architecture

While there are many different power system architectures, hybrid-electric aircraft in general combine the high specific energy storage of fuel with the increased efficiency of power electronics. In the particular *range extender* architecture, propulsion comes from an electrically-driven propeller allowing the aircraft

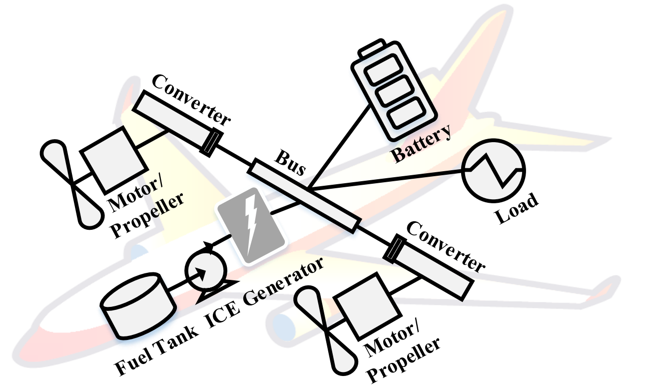

FIGURE 1. Candidate hybrid-electric aircraft power system architecture.

can fly for short periods using only electrical power. To overcome the relatively low specific energy of electrical batteries, this architecture also includes a fuel tank, an internal combustion engine (ICE), and an electric generator to create additional electricity to charge the battery and/or to directly power the electric motor. A detailed review of the state-of-the-art in the electrification of aircraft is provided in [18] and the references therein.

The specific hybrid-electric aircraft power system presented in this paper is shown in Fig. 1. This system consists of a single fuel tank and two parallel ICEs/generators to provide electrical power to the main electrical bus. This bus is connected to a battery pack that can be charged or discharged as needed. The bus provides electrical power to two parallel converters that control the power to each of the electric motors driving the propellers. A generic load is also attached to the bus representing internal electrical loads such as avionics or mission-payloads.

This particular system architecture was chosen to capture the primary power system components and energy management challenges associated with a wide variety of hybrid-electric aircraft. In particular, an effective controller must strategically charge and discharge the battery to achieve the desired aircraft performance while minimizing fuel consumption and regulating the fast underdamped dynamics in the electrical power system.

The dynamic models for each of the components in the system are based on the graph-based modeling and model validation efforts presented in [4, 19, 20]. The following section provides a brief overview of the graph-based modeling framework.

2.2 Graph-based Modeling

This paper employs graph-based modeling to capture how energy is stored and transferred in the multiple energy domains found in hybrid-electric aircraft power systems. Specifically, graph-based modeling of the candidate system shown in Fig. 1 captures the chemical energy stored in the fuel, rotational mechanical energy stored in the engines and motors, and the electrical energy stored in the battery and power electronics.

When capturing the structured dynamics of a system, a graph consists of a set of dynamic vertices $V = \{v_i : i \in [1, N_v]\}$, representing energy stored by capacitative elements of a system, and a set of edges $E = \{e_j : j \in [1, N_e]\}$, representing power flows among these capacitative elements. Each edge e_j has a orientation denoting the direction of positive power flow P_j from the tail vertex v_j^{tail} to the head vertex v_j^{head}. Based on conservation of energy, the energy stored by i^{th} vertex v_i (quantified by the dynamic state x_i) can be expressed as

$$C_i \dot{x}_i = \sum_{e_j \in E_i^{in}} P_j - \sum_{e_j \in E_i^{out}} P_j, \tag{1}$$

where C_i is the energy storage capacitance while E_i^{in} and E_i^{out} are the set of edges directed into and out of vertex v_i. Generally, in a graph-based modeling framework, the power flow P_j is constrained to be a function of an associated input $\tilde{u}_j$ and the state of the tail and head vertices, x_j^{tail} and x_j^{head}, such that

$$P_j = f_j(x_j^{tail}, x_j^{head}, \tilde{u}_j). \tag{2}$$

In general, the graph-based modeling framework allows for power to enter the system along source edges as discussed in [4]. However, for the aircraft system shown in Fig. 1, there is no source of power flow into the aircraft, so these source edges will be neglected in this paper. To allow power to exit the system in the form of heat loss due to inefficiencies in the mechanical and electrical systems and aerodynamic drag, a set of sink vertices denoted $V^{out} = \{v_i^{out} : i \in [1, N_v^{out}]\}$ are included in the graph. Each of these vertices has an associated state x_i^{out} that serves as a disturbance to the system.

The structure of the graph, including both the dynamic vertices and sink vertices, is captured by the incidence matrix $M = [m_{ij}] \in \mathbb{R}^{(N_v + N_v^{out}) \times N_e}$ defined as

$$m_{ij} = \begin{cases} +1 & \text{if } v_i \text{ is the tail of } e_j, \\ -1 & \text{if } v_i \text{ is the head of } e_j, \\ 0 & \text{else.} \end{cases} \tag{3}$$

The incidence matrix is partitioned based on dynamic and sink vertices such that

$$M = \begin{bmatrix} \bar{M} \\ \underline{M} \end{bmatrix} \text{ with } \bar{M} \in \mathbb{R}^{N_v \times N_e}, \tag{4}$$

where the indexing of vertices is assumed to be ordered such that $\bar{M}$ is a structural mapping from power flows

$$P = F(x, x^{out}, \tilde{u}) = [f_j(x_j^{tail}, x_j^{head}, \tilde{u}_j)], \tag{5}$$

to states $x = [x_i]$, $i \in [1, N_v]$, and $\underline{M}$ is a structural mapping from P to sink states $x^{out} = [x_i^{out}]$, $i \in [1, N_v^{out}]$. Combining the individual conservation equations from (1) using the structure of the graph captured by $\bar{M}$, the overall system dynamics are

$$C\dot{x} = -\bar{M}P = -\bar{M}F(x, x^{out}, \tilde{u}), \tag{6}$$

where $C = diag([C_i])$, $i \in [1, N_v]$ is a diagonal matrix of capacitances. Since some edges do not have a control input and a single input can affect multiple edges, it is often advantageous to let $\tilde{u} \in \mathbb{R}^{N_e}$ be a virtual input vector, corresponding to the N_e edges, and define $u \in \mathbb{R}^{N_u}$ as a system input vector, corresponding to the subset of N_u unique inputs that affect the system. As such, the matrix $\Phi \in \mathbb{R}^{N_e \times N_u}$ can be used to map the system inputs to the virtual inputs such that $\tilde{u} = \Phi u$.

One benefit of a graph-based modeling framework is that the linear structure of the graph is captured by (6) and the majority of the modeling effort focuses on defining the potentially nonlinear power flow relationships in (5). The following section presents the graph capturing the structure of the system shown in Fig. 1 and the vertex and edge properties used to model the dynamics.

2.3 Complete System Graph and Component Models

Fig. 2 shows the graph structure of the power system from Fig. 1. In total, the system graph has 16 vertices/states, 3 sink vertices, 32 edges/power flows, and 7 unique control inputs. The properties for each vertex and edge are summarized in Table 1 along the nominal values for states and inputs used for linearization and their upper- and lower-bounds that constraint system operation. These system parameters were chosen to represent a hybrid-electric aircraft similar in size to the UAV presented in [20]. Due to symmetry in the system, multiple vertices and edges have similar properties and thus the notation $v_{2,3}$ is used to refer to vertices v_2 and v_3. The individual component graph-models are based on similar formulations presented in [19] and [20]. The fidelity of the models used in this paper has been chosen to highlight the hierarchical MPC control design and the corresponding control performance on a dynamic system model that captures the fundamental power system dynamics of a hybrid-electric aircraft. In general, the validity of the graph-based modeling approach has been experimentally validated on a variety of power systems as detailed in [14, 19, 20]. It is intended that the models presented in this paper can be readily extended as necessary to capture behaviors found in a specific system without significant modification to the overall approach.

2.4 Linearization and Discretization

To apply the linear set-based hierarchical MPC developed in [16], the nonlinear continuous-time graph-based model must be linearized and discretized. The nonlinear dynamics of (6) are

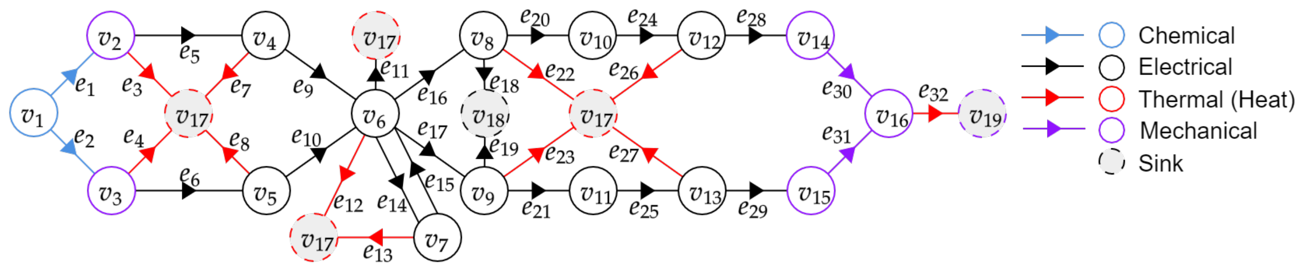

FIGURE 2. Graph representation of the power system from Fig. 1.

TABLE 1. SYSTEM VERTEX, EDGE, STATE, INPUT, AND PARAMETER DEFINITIONS.

Vertex	State	Variable	Units	Nominal Value	Lower Bound	Upper Bound	Capacitance
v_1	x_1	Fuel mass	kg	100	0	100	U
$v_{2,3}$	$x_{2,3}$	ICE shaft speed	rad/s	100	0	300	$J_e x_2$
$v_{4,5}$	$x_{4,5}$	Bus input current	A	20.7	0	62.1	$L_{bus} x_4$
v_6	x_6	Bus voltage	V	640.8	600	680	$C_{bus} x_6$
v_7	x_7	State of Charge	-	0.5	0	1	C_b
$v_{8,9}$	$x_{8,9}$	Converter current	A	50	0	150	$L_c x_8$
$v_{10,11}$	$x_{10,11}$	Converter voltage	V	255.4	0	766.2	$C_c x_{10}$
$v_{12,13}$	$x_{12,13}$	Motor current	A	50	0	150	$L_m x_{12}$
$v_{14,15}$	$x_{14,15}$	Prop. shaft speed	rad/s	230.4	0	691.2	$J_p x_{14}$
v_{16}	x_{16}	Aircraft velocity	m/s	40	25	60	$(M_{dry} + x_1) x_{16}$
v_{17}	x_{17}	Ambient temp.	°C	-	Sink state		
v_{18}	x_{18}	Diode voltage	V	80	Sink state		
v_{19}	x_{19}	Wind speed	m/s	0	Sink state		

Edge	Power Flow	Description
$e_{1,2}$	$P_1 = U u_1$	Fuel energy into ICE
$e_{3,4}$	$P_3 = (1-\eta_e) U u_1 + \alpha_e x_2$	ICE heat generation
$e_{5,6}$	$P_5 = K_g x_2 x_4$	Generator electrical power
$e_{7,8}$	$P_7 = R_{bus} x_4^2$	Bus heat generation
$e_{9,10}$	$P_9 = x_4 x_6$	Bus input power
e_{11}	$P_{11} = u_7$	Load power
e_{12}	$P_{12} = \frac{1-\eta_b}{\eta_b} u_5$	Battery charge heat generation
e_{13}	$P_{13} = (1-\eta_b) u_6$	Battery discharge heat generation
e_{14}	$P_{14} = u_5$	Battery charge power
e_{15}	$P_{15} = \eta_b u_6$	Battery discharge power
$e_{16,17}$	$P_{16} = x_6 x_8 u_3$	Converter input power
$e_{18,19}$	$P_{18} = x_8 x_{18} (1-u_3)$	Converter diode power
$e_{20,21}$	$P_{20} = x_8 x_{10}$	Converter internal power
$e_{22,23}$	$P_{22} = R_d x_8^2 (1-u_3)$	Converter heat generation
$e_{24,25}$	$P_{24} = x_{10} x_{12}$	Motor input power
$e_{26,27}$	$P_{26} = R_m x_{12}^2$	Motor heat generation
$e_{28,29}$	$P_{28} = K_m x_{12} x_{14}$	Propeller input power
$e_{30,31}$	$P_{30} = C_T \rho \left(\frac{x_{14}}{2\pi}\right)^2 D^4 x_{16}$	Propeller thrust
e_{32}	$P_{32} = \frac{1}{2} \rho A C_d (x_{16} - x_{19})^2 x_{16}$	Aerodynamic drag

Input	Variable	Units	Nominal Value	Lower Bound	Upper Bound
$u_{1,2}$	Fuel mass flow rate	kg/s	0.0025	0	0.005
$u_{3,4}$	Converter duty cycle	-	0.5	0	1
u_5	Charge power	kW	0	0	100
u_6	Discharge power	kW	10	0	100
u_7	Load power	kW	2.5	0	25

Parameter	Value	Units	Description
U	46000	kJ/kg	Calorific value of jet fuel
J_e	10	$kg \cdot m^2$	ICE mass moment of inertia
L_{bus}	1	H	Bus inductance
C_{bus}	1	F	Bus capacitance
C_b	100	MJ	Battery capacitance
L_c	1	H	Converter inductance
C_c	1	F	Converter capacitance
L_m	0.4	H	Propeller motor inductance
J_p	10	$kg \cdot m^2$	Propeller mass moment of inertia
M_{dry}	800	kg	Mass of aircraft without fuel
η_e	0.25	-	ICE efficiency
α_e	0.15	$kW/(rad/s)$	ICE friction coefficient
K_g	6.5115	$V \cdot s/rad$	Generator speed to voltage coeff.
R_{bus}	0.5	Ω	Bus input resistance
η_b	0.8	-	Battery efficiency
R_d	1	Ω	Diode resistance
R_m	0.5	Ω	Motor resistance
K_m	1	$V \cdot s/rad$	Motor constant
C_T	0.0061	-	Propeller thrust coefficient
ρ	0.9	kg/m^3	Air density
D	2.5	m	Propeller diameter
A	20	m^2	Aircraft reference area
C_d	0.04	-	Aircraft drag coefficient

linearized about nominal states x^o, sink states $x^{out,o}$, and inputs u^o. While linearization is typically performed about an equilibrium, for aircraft systems it is valuable to linearize about a nominal operation condition during flight where some states may not be at an equilibrium, such as the mass of fuel or battery SOC. Since all of the nonlinearities are captured in the power flow equations from (5), each edge can be linearized individually. Thus each power flow P_j is approximated as

$$P_j = f_j(x_j^{tail}, x_j^{head}, \tilde{u}_j) \approx a_j x_j^{tail} + b_j x_j^{head} + c_j \tilde{u}_j + d_j. \tag{7}$$

As in [21], let the weighted incidence matrix $\mathcal{M} = [m_{ij}] \in \mathbb{R}^{(N_v + N_v^{out}) \times N_e}$ be defined as

$$m_{ij} = \begin{cases} a_j & \text{if } v_i \text{ is the tail of } e_j, \\ b_j & \text{if } v_i \text{ is the head of } e_j, \\ 0 & \text{else.} \end{cases} \tag{8}$$

Then the vector of linearized power flows is expressed as

$$P = \mathcal{M}^T \begin{bmatrix} x \\ x^{out} \end{bmatrix} + \beta \tilde{u} + d = \bar{\mathcal{M}}^T x + \underline{\mathcal{M}}^T x^{out} + \beta \tilde{u} + d, \tag{9}$$

where $\beta = diag([c_j])$ and $d = [d_j]$. Combining (6) and (9), the linearized continuous-time dynamics are

$$C\dot{x} = -\bar{M}\bar{\mathcal{M}}^T x - \bar{M}\beta\Phi u - \bar{M}\underline{\mathcal{M}}^T x^{out} - \bar{M}d. \tag{10}$$

Using a zero-order hold, the continuous dynamics of (10) can be discretized to get the discrete-time state-space model

$$x(k+1) = Ax(k) + Bu(k) + Vw(k) + c, \tag{11}$$

with states $x \in \mathbb{R}^{16}$, inputs $u \in \mathbb{R}^7$, disturbances $w \in \mathbb{R}^3$, and constant vector $c \in \mathbb{R}^{16}$ due to the linearization.

Fig. 3 shows an open-loop comparison between the linearized model (11) and the nonlinear graph-based model (6) for several representative states based on step input changes. The linear system is discretized with a time step size of $\Delta t = 1$ second. While the linearization and discretization introduce some model error, the key transient and steady-state dynamics are sufficiently captured by the linear model. Therefore, the following set-based hierarchical MPC formulation is developed using the linear model and applied to the linear model. Future work will focus on systematically quantifying the linearization and discretization error and using these error bounds to formulate a robust set-based hierarchical MPC as in [17].

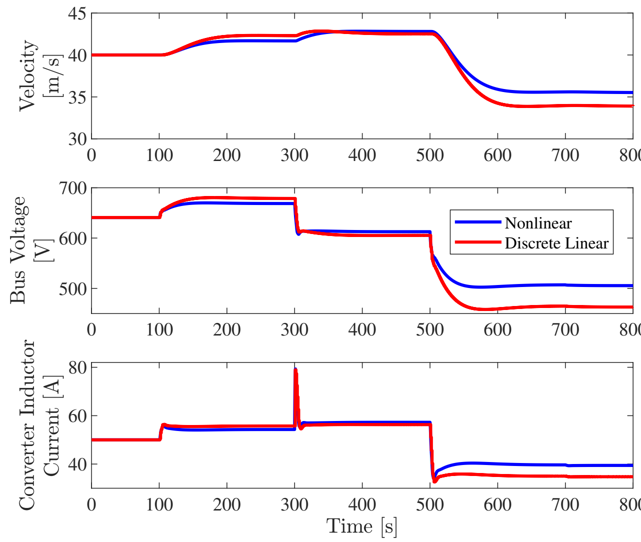

FIGURE 3. Simulation results comparing the continuous-time nonlinear aircraft model and discrete-time linear aircraft model.

3 SET-BASED HIERARCHICAL MPC

As discussed in [15], the goals for any aircraft energy management controller are to 1) maximize the capability of the aircraft by achieving the desired operation of mission- and flight-critical hardware; 2) satisfy various system constraints for safe and reliable operation; and 3) minimize fuel consumption. To achieve these goals, this paper uses the notion of mission-based MPC presented in [22]. Under the assumption of finite operation, the discrete-time linear system (11) starts at an initial condition of $x(0)$ at time $t = 0$ and operates with a fixed time step size Δt until the end of operation at $t = t_F = k_F \Delta t$. The discrete time steps for system operation are indexed by $k = [0, k_F]$. Within the mission-based MPC framework, the primary control objective is to plan and execute an input trajectory $\{u(k)\}_{k=0}^{k_F - 1}$ and corresponding state trajectory $\{x(k)\}_{k=0}^{k_F}$ subject to (11) that satisfy the operating and terminal constraints

$$x(k) \in \mathcal{X} \subset \mathbb{R}^n, u(k) \in \mathcal{U} \subset \mathbb{R}^m, \forall k \in [0, k_F - 1], \tag{12}$$

$$x(k_F) \in \mathcal{T} \subseteq \mathcal{X}. \tag{13}$$

The secondary control objective is to minimize the cost function

$$J^*(x(0)) = \min_{\{u(k)\}_{k=0}^{k_F-1}} \sum_{j=0}^{k_F} \ell(x(j), u(j), r(j)), \tag{14}$$

where the pre-determined reference trajectory $\{r(k)\}_{k=0}^{k_F}$ defines the desired system operation.

While a centralized MPC approach that predicts over the entire remainder of system operation represents the optimal solution to this control problem, small time steps Δt and long missions lengths t_F often make a centralized solution impractical due to high computational costs. This is particularly true for systems with a large number of states and inputs.

Therefore, for energy management of a hybrid-electric aircraft, this paper uses a two-level vertical hierarchical MPC formulation based on set-based hierarchical MPC from [16]. The upper-level controller is denoted as C_1 and the lower-level controller is denoted as C_2. By decomposing control decisions among two levels, the upper-level controller can focus on planning long-term state trajectories over the entire reminder of system operation while the lower-level controller can refine these long-term state trajectories with a faster control update rate that accounts for the fast dynamics of the system. The lower-level controller C_2 has the same time step size as (11), such that $\Delta t_2 = \Delta t$. The choice of prediction horizon of C_2 and the time step size of C_1 are coordinated such that C_2 only predicts between consecutive updates of C_1. Therefore, the slow time step size of C_1 is chosen such that $\Delta t_1 = N_2 \Delta t_2$, where N_2 is the prediction horizon of the lower-level controller. Since C_1 is designed to predict to the end of system operation, the upper-level prediction horizon is chosen as $N_1 = \frac{t_F}{\Delta t_1}$. Let, $\nu_1 = \frac{\Delta t_1}{\Delta t}$ be the time scaling factor for C_1. As such, the time steps for C_1 are indexed by $k_1 \in [0, k_{1,F}]$, where $k_{1,F} = \frac{k_F}{\nu_1}$, while the time steps for C_2 are indexed by $k_2 = k \in [0, k_F]$. While additional details and theoretical analysis of set-based hierarchical MPC can be found in [16] and [17], the following sections present the main ideas and formulation of set-based hierarchical MPC to be used for the energy management of hybrid-electric aircraft.

3.1 MPC Formulation

At every large time step, C_1 solves the constrained optimization problem

$$J_1^*(x(k)) = \min_{U_1(k_1)} \sum_{j=k_1}^{k_{1,F}} \ell\left(x_1(j|k_1), u_1(j|k_1), r_1(j)\right), \tag{15a}$$

$$\begin{aligned}
&\text{s.t.} \, \forall j \in [k_1, k_{1,F}] \\
&\quad x_1(j+1|k_1) = A_1 x_1(j|k_1) + B_1 u_1(j|k_1) + c_1, && \text{(15b)}\\
&\quad x_1(j|k_1) \in \mathcal{X}_1,\, u_1(j|k_1) \in \mathcal{U}_1, && \text{(15c)}\\
&\quad x_1(k_{1,F}|k_1) \in \mathcal{T}, && \text{(15d)}\\
&\quad x_1(k_1|k_1) = x(k) \vee x_1^*(k_1|k_1-1). && \text{(15e)}
\end{aligned}$$

First, note that C_1 has a *shrinking horizon*, based on the summation limits in (15a). This allows C_1 to predict to the end of system operation. The input sequence over this horizon is defined as $U_1(k_1) = \{u_1(j|k_1)\}_{j=k_1}^{k_{1,F}-1}$. In (15b), the model used by C_1 assumes a piecewise constant control input over the time step Δt_1 and thus $A_1 = A^{\nu_1}$ and $B_1 = \sum_{j=0}^{\nu_1-1} A^j B$ (as in [23]). Additionally, the constant $c_1 = \sum_{j=0}^{\nu_1-1} A^j (Vw + c)$ is computed assuming the disturbances $w(k)$ in (11) are constant. In (15c), the states and inputs are constrained to the tightened constraint sets $\mathcal{X}_1$ and $\mathcal{U}_1$. In (15d), the terminal constraint from (13) is imposed. Finally, (15e) provides C_1 the choice of initial condition, $x_1(k_1|k_1)$, as either the current state of the system, $x(k)$, or the optimal state at this time step determined by C_1 at the previous time step, $x_1^*(k_1|k_1-1)$. This initial condition option is a technical requirement for guaranteed feasibility as discussed in detail in [16].

While the formulation of the lower-level controller is very similar, the following highlights the key differences. At every time step of the discrete system, C_2 solves the constrained optimization problem

$$J_2^*(x(k)) = \min_{U(k_2)} \sum_{j=k_2}^{k_2+N_2(k_2)} \ell\left(x(j|k_2), u(j|k_2), r(j)\right), \tag{16a}$$

$$\begin{aligned}
&\text{s.t.} \, \forall j \in [k_2, k_2+N_2(k_2)] \\
&\quad x(j+1|k_2) = Ax(j|k_2) + Bu(j|k_2) + Vw + c, && \text{(16b)}\\
&\quad x(j|k_2) \in \mathcal{X},\, u(j|k_2) \in \mathcal{U}, && \text{(16c)}\\
&\quad x(k_2+N_2(k_2)|k_2) \in \mathcal{S}_2(k_2+N_2(k_2)), && \text{(16d)}\\
&\quad x(k_2|k_2) = x(k). && \text{(16e)}
\end{aligned}$$

The lower-level controller has a *resetting shrinking horizon* with horizon length $N_2(k_2) \triangleq N_2 - (k_2 \mod N_2)$. Thus, C_2 always predicts to the next update of C_1, at which point the prediction horizon resets. Coordination between C_1 and C_2 is achieved using the wayset-based terminal constraint imposed in (16d). The following sections provide the main ideas behind the formulation of the tightened output constraint sets and waysets along with their roles in guaranteeing output and terminal constraint satisfaction with additional details found in [16].

3.2 Constraint Tightening

A fundamental feature of set-based hierarchical MPC is that the trajectory determined by the upper-level controller C_1 is always a feasible candidate trajectory for the lower-level controller C_2. However, due to the large time step size Δt_1, C_1 only predicts state trajectories at the slow time step indices k_1 and is unaware of the states at the inter-sample time steps $k \in [\nu_1 k_1 + 1, \nu_1(k_1+1) - 1]$. Therefore, in the formulation of C_1, tightened state and input constraint sets $\mathcal{X}_1$ and $\mathcal{U}_1$ are used to impose additional constraints based on this inter-sample behavior. While the exact procedure for computing $\mathcal{X}_1$ and $\mathcal{U}_1$ is presented in [16], the key idea is to place constraints on $x_1(k_1)$ and $u_1(k_1)$ such that the inter-sample state trajectory based on a zero-order hold of $u_1(k_1)$ remains within the state constraint set.

3.3 Wayset

As previously mentioned, the wayset imposed as a terminal constraint for the lower-level controller in (16d) provides the only coordination between controllers C_1 and C_2. While the idea of a wayset is highly generalizable, set-based hierarchical MPC relies on formulating waysets $\mathcal{S}(k) \subset \mathcal{X}$ that represent a set of states at time step k such that for any $x(k) \in \mathcal{S}(k)$ there exists a future input trajectory $\{u(j)\}_{j=k}^{k_F-1}$ and corresponding state trajectory $\{x(j)\}_{j=k}^{k_F}$ that satisfy the state, input, and terminal constraints from (12) and (13).

Since computing these waysets must be performed online immediately following every update of the upper-level controller C_1, the computational efficiency of generating waysets is critical to the overall applicability of set-based hierarchical MPC. Therefore, [16] employed constrained zonotopes, first developed in [24], as an extremely efficient method for computing the linear transformations, Minkowski sums, and set intersections required to compute waysets.

By representing waysets as constrained zonotopes, each wayset $\mathcal{S}$ is defined in constrained generator-representation (CG-Rep) where $\mathcal{S} = \{G\xi + c \mid \|\xi\|_\infty \leq 1, A\xi = b\}$. This set is defined by its center $c \in \mathbb{R}^n$ and n_g generators g_i that form the columns of $G \in \mathbb{R}^{n \times n_g}$. Constrained zonotopes also have n_c equality constraints on ξ, where $A \in \mathbb{R}^{n_c \times n_g}$ and $b \in \mathbb{R}^{n_c}$, which allow any convex polytope to be represented in CG-Rep [24].

While zonotopes avoid the potential exponential growth in complexity associated with more conventional polytopic set representations, the number of generators still grows linearly with the number of discrete steps taken when computing the wayset. Assuming $\mathcal{X}$ and $\mathcal{U}$ are defined with box constraints for the n states and m inputs, then the total number of generators needed to represent the wayset is $n_g = (n+m)N_2$, where N_2 is the prediction horizon of the lower-level controller [17]. As will be discussed in Section 4, a prediction horizon of $N_2 = 25$ steps along with the $n = 16$ states and $m = 7$ inputs results in $n_g = 575$ generators. Since, the number of constraints imposed by the wayset terminal constraint condition in (16d) directly affects the computational cost of solving C_2, reducing the total number of generators required to represent $\mathcal{S}(k)$ may become necessary in certain applications. Therefore, Fig. 4 shows an alternative method for computing $\mathcal{S}(k)$ where the input determined by C_1 is used for a user-defined number of steps N_0, with the effect of reducing the number of generators to $n_g = (n+m)(N_2 - N_0)$. While this reduces the overall computational complexity of C_2, Fig. 4 also shows how this reduces the size of the wayset and thus reduces the flexibility of C_2 to deviate from the trajectory determined by C_1. However, as shown in the numerical results in Section 4, even setting $N_0 = N_2 - 1$ such that $n_g = 23$ still provides enough flexibility to produce the required control performance with significantly less computational cost.

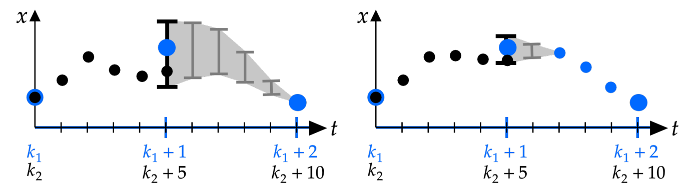

FIGURE 4. To reduce wayset complexity, the approach from [16] shown on the left can be modified as shown on the right with $N_2 = 5$ and $N_0 = 3$. The large blue dots represent the planned state trajectory from C_1, the gray regions show the backward reach set approach to computing waysets, the small black dots represent the planned state trajectory by C_2 with the wayset terminal constraint, and the small blue dots represent the state trajectory achieved by applying the input determined by C_1 for N_0 steps in order to reduce the complexity of the wayset.

3.4 Controller Guarantees

In addition to the number of practical control benefits provided by wayset-based coordination, set-based hierarchical MPC is one of the few hierarchical MPC approaches that can guarantee state and input constraint satisfaction. Specifically, for the controller formulations presented in Section 3.1, the upper-level constraint tightening in Section 3.2, and the wayset computations in Section 3.3, both controllers C_1 and C_2 are guaranteed to have feasible solutions at every time step with resulting system trajectories that satisfy the state, input, and terminal constraints from (12) and (13). The detailed explanation and proof of this claim is provided in [16] for nominal system dynamics without disturbances and in [17] where the MPC formulations are made robust to unknown bounded disturbances. While the following section focuses on the control performance of the two-level set-based hierarchical MPC applied to the hybrid-electrical aircraft system from Section 2, note that all state and input constraints are satisfied at all time steps as a results of the theory that supports this specific hierarchical control formulation.

4 NUMERICAL RESULTS

To demonstrate the benefits of set-based hierarchical MPC for the control of hybrid-electric aircraft power systems, the performance of the hierarchical controller is tested for a mission length of 1 hour ($t_F = 3600$ seconds) representative of a mid-flight segment of operation. With a discrete time step of $\Delta t = \Delta t_2 = 1$ second, the lower-level controller C_2 is designed with a maximum prediction horizon of $N_2 = 25$ steps. Thus the upper-level controller C_1 has a constant time step size of $\Delta t_1 = 25$ seconds and an initial prediction horizon of $N_1 = 144$ steps, which shrinks during operation as discussed in Section 3.1. The initial condition $x(0)$ is taken as the nominal value used for linearization as provided in Table 1. As with mission-based MPC [22], the primary objective is to satisfy all state and input

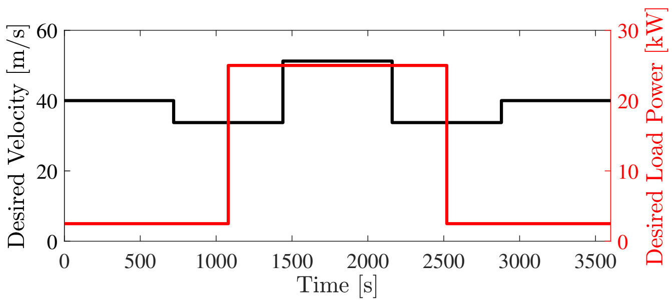

FIGURE 5. References for aircraft velocity and load power.

constraints during operation, listed in Table 1, and a set of terminal constraints at the end of operation. For this work, $\mathcal{T} = \mathcal{X}$. Satisfying this primary objective is guaranteed by the set-based hierarchical MPC formulation and is confirmed by the following results. The secondary objective is to achieve the desired system operation, which is defined by minimizing the cost function from (14) taken to be the weighted quadratic cost function

$$\ell(x(j), u(j), r(j)) = \|r(j) - y_r(j)\|_\Lambda^2 + \ell_{\Delta_x} + \ell_{\Delta_u}. \qquad (17)$$

Here y_r represents a subset of states and outputs for which there are references. In this work, y_r consists of the aircraft velocity x_{16}, bus voltage x_6, fuel mass flow rates u_1, u_2, and load power u_7. With constant references of zero to minimize fuel mass flow rate and 640 volts to regulate the bus voltage, the time-varying references for velocity and load power are shown in Fig. 5. The weighting term $\Lambda = \mathrm{diag}\left([10^1\ 10^1\ 10^{-3}\ 10^{-3}\ 10^3]\right)$ assigns relative priority to the five reference tracking objectives. Note that due to the large range in signal magnitudes seen by the nominal state and input values in Table 1, all states and input are scaled to be between zero and one when formulating and solving the MPC optimization problems. Thus Λ reflects the relative weights on the scaled states and inputs. Also note that 14 of 16 states and 4 of 7 inputs are not provided references and the controller is tasked with utilizing these states to best track the five provided references. Given this high-degree of flexibility and large number of optimization variables in each MPC formulation, the cost function (17) also includes the terms

$$\ell_{\Delta_x} + \ell_{\Delta_u} = \|x(j+1) - x(j)\|_{\Lambda_x}^2 + \|u(j) - u(j-1)\|_{\Lambda_u}^2, \qquad (18)$$

which penalize the rate of change for each state and input where both Λ_x and Λ_u are diagonal matrices of ones except with $\Lambda_u(7,7) = 0.1$ to permit rapid changes in the load power. The inclusion of these rate penalties significantly reduces unnecessary oscillation in closed-loop system behavior.

In addition to the state, input, and terminal constraints included in (15) and (16), both controllers are also formulated with

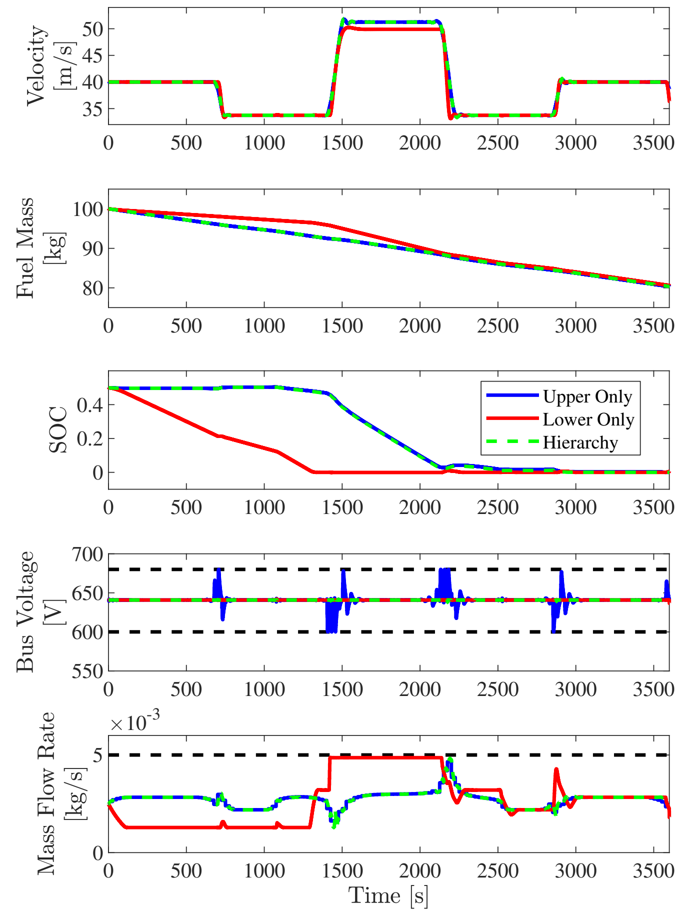

FIGURE 6. Simulation results comparing the two-level set-based hierarchical controller to benchmark MPC formulations where only the upper-level or lower-level controllers are used.

logical constraints such that the system is either charging or discharging the battery, but not both, at any point in time. The addition of these constraints turns (15) and (16) from Quadratic Programs (QPs) to mixed-integer Quadratic Programs (MIQPs). Despite advances in the ability to solve MIQPs rapidly, the transition from QPs to MIQPs results in a significant increase in computational cost due to the relatively long prediction horizons of both controllers. Therefore, to remain practical, each controller is formulated with the binary charging/discharging constraint for only the first step in the prediction horizon. This guarantees that the battery is never charged and discharged simultaneously and significantly reduces computational cost.

Fig. 6 shows the simulation results of the two-level hierarchical controller applied to the linearized and discretized aircraft model based on the nominal values provided in Table 1 compared to two benchmark MPC formulations. The first benchmark (Upper Only) corresponds to applying the control inputs determined by the upper-level controller C_1 directly to the system to high-

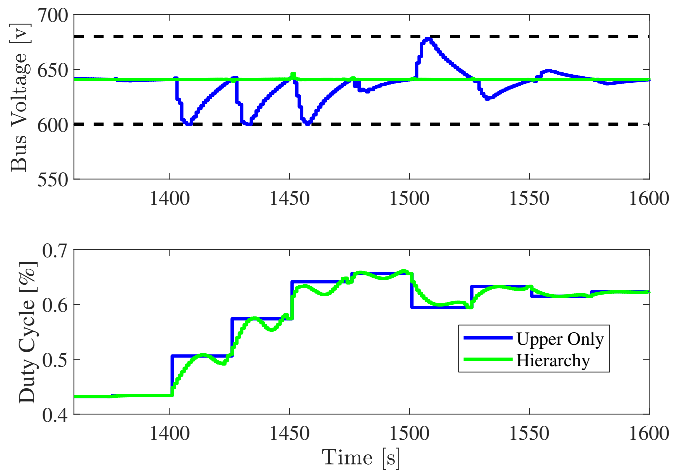

FIGURE 7. Comparison of the hierarchical and Upper Only controllers showing how the lower-level controller in the hierarchy is able to improve bus voltage regulation by deviating from the converter duty cycle input trajectory planned by the upper-level controller.

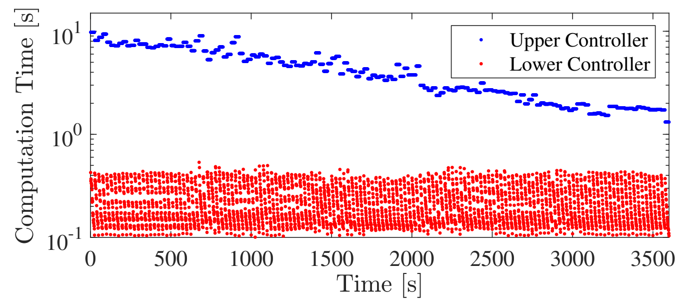

FIGURE 8. Computation times required to solve the upper-level and lower-level controllers in the hierarchy.

light the value of including the lower-level controller C_2 in the hierarchy. The second benchmark (Lower Only) corresponds to a more conventional short-horizon ($N = 25$ steps) centralized MPC controller with the same update rate as C_2 to highlight the value of the wayset-based guidance provided to C_2 by C_1 in the hierarchical formulation. The first subplot shows that the hierarchy and Upper Only controllers can track the desired references very well while the Lower Only controller is unable to track the velocity reference during the high-speed phase. The second and third subplots show that the Lower Only controller uses the battery too early while the hierarchy and Upper Only controllers reserve the battery for use during the high-speed phase. The fourth subplot shows how the Upper Only controller is unable to regulate the fast bus voltage dynamics. With the ability to deviate from the planned upper-level trajectory, the lower-level controller in the hierarchy is able to significantly improve this voltage regulation. The fifth subplot shows the effect of using the battery too early where the fuel mass flow rate saturates at the upper bound causing the high-speed velocity tracking error by the Lower Only controller seen in the first subplot.

An important feature of set-based hierarchical MPC is that wayset-based coordination allows the lower-level controller to significantly deviate from the input trajectory determined by the upper-level control to *use* the fast dynamics of the system to further improve performance. This behavior is highlighted by focusing on a 240 second portion of the 3600 second operation as shown in Fig. 7

Fig. 8 shows the computation times required to solve the upper- and lower-level controller optimization problems. Note that computation time required to solve the upper-level controller is much more than lower-level controller because of the large difference in prediction horizons ($N_1 = 144$, $N_2 = 25$). However, all computation times are less than the time step size for each controller, and thus this hierarchical controller is capable of executing in real-time. Note that the controller computation times are roughly an order-of-magnitude larger than those shown in Fig. 8 if the battery charging/discharging constraint is included for every step in the prediction horizon, resulting in computations times that exceed the controller time steps. While not shown, the computation of waysets is on the order of 1-10 milliseconds due to the use of constrained zonotopes. All results were generated using MATLAB on a desktop computer with a 3.6 GHz i7 processor and 16 GB of RAM and all MPC optimization problems were formulated and solved with YALMIP [25] and Gurobi [26].

5 CONCLUSION

A two-level set-based hierarchical MPC formulation was presented for the control of hybrid-electric aircraft. Graph-based modeling was used to capture the key components and dynamic behavior of the power systems for a range extender architecture. After deriving a linear discrete-time representation of the system dynamics, a set-based hierarchical MPC formulation was presented which enables guaranteed satisfaction of input and state constraints throughout system operation. Waysets were used to coordinate the upper- and lower-level MPC controllers of the hierarchy as a computationally efficient way to combine the benefits of a long prediction horizon and a fast control update rate. Simulation results show both the performance benefits of hierarchical control of aircraft power systems as well as the practicality of set-based hierarchical control for a system with 16 states and 7 inputs. Future work will focus on quantifying linearization and discretization error to develop a robust set-based hierarchical MPC for hybrid-electric aircraft power systems with greater model fidelity.

ACKNOWLEDGMENT

This material is based upon work supported by the National Science Foundation under Grant No. 1849500.

REFERENCES

[1] Camacho, E. F., and Bordons, C., 2007. *Model Predictive Control*, 2nd ed. Springer.

[2] Roberts, R. A., and Eastbourn, S. M., 2014. "Vehicle Level Tip-to-Tail Modeling of an Aircraft". *International Journal of Thermodynamics,* ***17***(2).

[3] Williams, M., Sridharan, S., Banerjee, S., Mak, C., Pauga, C., Krein, P., Alleyne, A., Jacobi, A., and D'Urso, S., 2015. "PowerFlow: A Toolbox for Modeling and Simulation of Aircraft Systems". *SAE Technical Paper 2015-01-2417*.

[4] Williams, M. A., Koeln, J. P., Pangborn, H. C., and Alleyne, A. G., 2018. "Dynamical Graph Models of Aircraft Electrical, Thermal, and Turbomachinery Components". *Journal of Dynamic Systems, Measurement, and Control,* ***140***.

[5] Falck, R. D., Chin, J. C., Schnulo, S. L., Burt, J. M., and Gray, J. S., 2017. "Trajectory optimization of electric aircraft subject to subsystem thermal constraints". *AIAA/ISSMO Multidisciplinary Analysis and Optimization Conference*.

[6] Huang, G. P., Doman, D. B., Rothenberger, M. J., Hencey, B., DeSimio, M. P., Tipton, A., and Sigthorsson, D. O., 2019. "Dimensional Analysis, Modeling, and Experimental Validation of an Aircraft Fuel Thermal Management System". *Journal of Thermophysics and Heat Transfer,* ***33***(4).

[7] Pangborn, H. C., Hey, J. E., Deppen, T. O., Alleyne, A. G., and Fisher, T. S., 2017. "Hardware-in-the-Loop Validation of Advanced Fuel Thermal Management Control". *Journal of Thermophysics and Heat Transfer,* ***31***(4).

[8] Seok, J., Kolmanovsky, I., and Girard, A., 2017. "Coordinated Model Predictive Control of Aircraft Gas Turbine Engine and Power System". *Journal of Guidance, Control, and Dynamics,* ***40***(10).

[9] Dunham, W., Hencey, B., Kolmanovsky, I., and Girard, A., 2019. "Scenario based stochastic MPC for more electric aircraft coordinated engine and power management". *American Control Conference*, pp. 4223–4228.

[10] Maasoumy, M., Nuzzo, P., Iandola, F., Kamgarpour, M., Sangiovanni-Vincentelli, A., and Tomlin, C., 2013. "Optimal Load Management System for Aircraft Electric Power Distribution". *IEEE Conference on Decision and Control*, pp. 2939–2945.

[11] Dunham, W., Hencey, B., Girard, A., and Kolmanovsky, I., 2017. "Distributed MPC via ADMM for Coordination and Control of More Electric Aircraft Subsystems". *ASME Dynamic Systems and Control Conference*.

[12] Dunham, W., Hencey, B., Girard, A. R., and Kolmanovsky, I., 2019. "Distributed Model Predictive Control for More Electric Aircraft Subsystems Operating at Multiple Time Scales". *IEEE Transactions on Control Systems Technology*.

[13] Pangborn, H. C., Williams, M. A., Koeln, J. P., and Alleyne, A. G., 2017. "Graph-based hierarchical control of thermal-fluid power flow systems". *American Control Conference*.

[14] Pangborn, H. C., Koeln, J. P., Williams, M. A., and Alleyne, A. G., 2018. "Experimental Validation of Graph-Based Hierarchical Control for Thermal Management". *Journal of Dynamic Systems, Measurement and Control,* ***140***.

[15] Koeln, J. P., Pangborn, H. C., Williams, M. A., Kawamura, M. L., and Alleyne, A. G., 2019. "Hierarchical Control of Aircraft Electro-Thermal Systems". *IEEE Transactions on Control Systems Technology*.

[16] Koeln, J. P., and Hencey, B. M., 2019. "Constrained Hierarchical MPC via Zonotopic Waysets". *American Control Conference*, pp. 4237–4244.

[17] Koeln, J. P., Raghuraman, V., and Hencey, B. M., 2020. "Vertical hierarchical MPC for constrained linear systems". *Automatica,* ***113***.

[18] Brelje, B. J., and Martins, J. R., 2019. "Electric, hybrid, and turboelectric fixed-wing aircraft: A review of concepts, models, and design approaches". *Progress in Aerospace Sciences,* ***104***, pp. 1–19.

[19] Williams, M. A., 2017. "A Framework for the Control of Electro-Thermal Aircraft Power Systems". *Ph.D. Dissertation, Dept. Mech. Eng., Univ. Illinois Urbana-Champaign, Urbana, IL.*

[20] Aksland, C. T., Bixel, T. W., Raymond, L. C., Rottmayer, M. A., and Alleyne, A. G., 2019. "Graph-based electro-mechanical modeling of a hybrid unmanned aerial vehicle for real-time applications". *American Control Conference*, pp. 4253–4259.

[21] Koeln, J., and Alleyne, A., 2018. "Robust hierarchical model predictive control of graph-based power flow systems". *Automatica,* ***96***, pp. 127–133.

[22] Koeln, J. P., and Alleyne, A. G., 2018. "Two-Level Hierarchical Mission-Based Model Predictive Control". *American Control Conference*.

[23] Scattolini, R., and Colaneri, P., 2007. "Hierarchical model predictive control". *IEEE Conference on Decision and Control*, pp. 4803–4808.

[24] Scott, J. K., Raimondo, D. M., Marseglia, G. R., and Braatz, R. D., 2016. "Constrained zonotopes: A new tool for set-based estimation and fault detection". *Automatica,* ***69***, pp. 126–136.

[25] Lofberg, J., 2004. "YALMIP: a toolbox for modeling and optimization in MATLAB". *2004 IEEE International Conference on Computer Aided Control Systems Design*.

[26] Gurobi Optimization, L. L. C., 2016. Gurobi Optimizer Reference Manual.